

# Evidence for excitonic insulator ground state in triangulene

## Kagome lattice

**Aidan Delgado<sup>1,†</sup>, Carolin Dusold<sup>1,†</sup>, Jingwei Jiang<sup>2,3,†</sup>, Adam Cronin<sup>1</sup>, Steven G. Louie<sup>2,3,\*</sup>**

**& Felix R. Fischer<sup>1,3,4,5,\*</sup>**

<sup>1</sup>Department of Chemistry, University of California, Berkeley, CA 94720, USA. <sup>2</sup>Department of Physics, University of California, Berkeley, CA 94720, USA. <sup>3</sup>Materials Sciences Division, Lawrence Berkeley National Laboratory, Berkeley, CA 94720, USA. <sup>4</sup>Kavli Energy NanoScience Institute at the University of California Berkeley and the Lawrence Berkeley National Laboratory, Berkeley, California 94720, USA.

<sup>5</sup>Baker Institute of Digital Materials for the Planet, Division of Computing, Data Science, and Society, University of California, Berkeley, CA 94720, USA.

<sup>†</sup> These authors contributed equally to this work.

\* Corresponding authors

Electron-hole pair excitations in semiconductors have been predicted to be able to give rise to a highly correlated many-body ground state, the excitonic insulator (EI)<sup>1,2</sup>. Under appropriate conditions below a critical temperature ( $T_c$ ), strongly bound electron-hole pairs spontaneously form and undergo a phase transition from a normal band insulator into an exciton condensate, transforming the parent material into a novel correlated insulator. Despite recent advances in spectroscopic tools, clear direct experimental evidence for the EI state has been elusive and is often obfuscated by accompanying electronic effects<sup>3-13</sup>. Here we present the reticular bottom-up synthesis of a Kagome lattice of [4]triangulene<sup>14</sup>, a two-dimensional (2D) covalent organic framework (COF) imbued with a deliberate excitonic instability<sup>15</sup> — excitons with binding energies larger than the bandgap — arising from a pair of flat bands (FBs). Theoretical analyses based on first-principles calculations and scanning tunnelling spectroscopy (STS) reveal quasiparticle spectral signatures mixing valence (VB) and conduction (CB) characteristics of the FBs along with a non-trivial semiconducting gap that can only be explained by invoking many-body theory<sup>16,17</sup>. Our findings spectroscopically corroborate the nature of a FB induced exciton insulator ground state and provide a robust yet highly tuneable platform for the exploration of correlated quasi boson physics in quantum materials.

A distinguishing characteristic of strongly correlated phases of matter is that the behavior of their constituent electronic excitations can no longer be described as a non-interacting renormalized *Fermi* gas. It is these correlated phases that have given rise to some of the most exciting quantum phenomena in materials. Excitonic insulators (a condensed phase of electron-hole pairs) is a correlated many-body ground state predicted in the 1960's that can arise in appropriate semimetals or narrow-gap semiconductors below a critical temperature ( $T_c$ )<sup>1,2,15,18</sup>. Whereas the high charge carrier density associated with the overlapping conduction and valence band (i.e., a negative band gap ( $E_g$ )) in semimetals effectively screens the electron-hole ( $e^-h^+$ ) interaction depressing  $T_c$ , an intrinsic instability in the single-particle (quasiparticle) band structure of a semiconductor can induce the spontaneous condensation of excitons — the electron-hole pairs — provided the exciton binding energy ( $E_b$ ) exceeds the magnitude of the gap in the conventional band insulator phase<sup>16,18-20</sup>. While the underlying principle has been understood for more than 50 years<sup>1,2</sup>, exercising a deterministic control over subtle many-body interactions represents a veritable challenge and could imbue otherwise ordinary materials with truly exotic electronic phases<sup>3-12,16,17,21-26</sup>. The realization of an EI could expand the boundaries of tailor-made quantum materials, providing deeper insight into strongly correlated phenomena, e.g. the crossover between Bardeen Cooper-Schrieffer (BCS) and BEC theory<sup>5,27,28</sup>.

Favourable conditions for the realization of an EI ground state ( $E_b > E_g$ ) not only call for small gap semiconductors, but for an increase in the quasiparticle masses and a reduction in the screening of the Coulomb potential binding the  $e^-h^+$  pairs — thus maximizing  $E_b$ . Layer materials herein represent privileged scaffolds as the 2D confinement intrinsically lowers the screening of charge carriers when compared to a 3D crystal lattice. The correlation between  $e^-$  and  $h^+$  can further be augmented by applying the tools of zero-mode engineering<sup>29</sup> to give rise to topological flat bands featuring charge carriers with huge effective masses and a greatly enhanced localization of the exciton wavefunction<sup>30-32</sup>. Our strategy for engineering a robust EI ground state follows the design of a diatomic Kagome lattice of triangulenes — nanoscale equilateral triangles of graphene cut along the  $a_1$  and  $a_2$  lattice vectors — proposed by Sethi *et al.*<sup>15,18</sup>. Fig. 1a shows a valence bond model for the open-shell  $S = 3/2$  ground state of an isolated [4]triangulene arising from a sublattice imbalance  $\Delta N = N_A - N_B = 3$ , where  $N_A$  and  $N_B$  are the number of

A and B sublattice sites of graphene, respectively. Nearest-neighbour analyses reveal three states (zero-modes) at the Fermi level. These three zero-modes unique to [4]triangulene are reminiscent of the orbital coordination number of a site in a diatomic Kagome lattice and when fused along the three vertices give rise to an orbital valence bond solid depicted in Fig. 1b ( $b_1$  and  $b_2$  are the lattice vectors of the diatomic Kagome lattice unit cell containing a pair of [4]triangulene superatoms). The corresponding tight-binding (TB) Hamiltonian can be expressed as

$$\hat{H} = t_1 \sum_{\langle ij \rangle \alpha} c_{i\alpha}^\dagger c_{j\alpha} + t_2 \sum_{\langle\langle ij \rangle\rangle \alpha} c_{i\alpha}^\dagger c_{j\alpha} + t_3 \sum_{\langle\langle\langle ij \rangle\rangle\rangle \alpha} c_{i\alpha}^\dagger c_{j\alpha} \quad (1)$$

where  $t_1$ ,  $t_2$ , and  $t_3$  are the hopping amplitudes defined in Fig. 1b ( $t_2$  is expected to be small due to sublattice polarization of the zero-modes).  $c_{i\alpha}^\dagger$  and  $c_{j\alpha}$  are the creation and annihilation operators of the zero-mode at site  $i$  and  $j$  with spin  $\alpha$ . The first term in Eq. 1 describes the hopping across a junction formed by fusing two triangulenes along their corners while the second and third terms correspond to the hopping within a single triangulene and the second nearest neighbour interaction between orbitals on two adjacent triangulenes, respectively. The TB Hamiltonian gives rise to six bands, a pair of valence (VB) and conduction (CB) FBs (blue and red bands in Fig. 1c, respectively) flanked on either side by pairs of comparatively dispersive bands. The large effective masses of and the overlap between  $e^-$  and  $h^+$  wavefunctions associated with the FBs in 2D increases the  $E_b$  while a large exchange interaction raises the singlet-triplet splitting energy ( $\Delta E_{ST}$ ) favouring the formation of a robust triplet EI ground state<sup>30-35</sup>, which are confirmed by our *ab initio* GW-BSE calculations<sup>33</sup> and in agreement with Sethi *et al.*<sup>15</sup>.

Guided by this idea we designed two competent molecular precursors for the reticular growth of a [4]triangulene COF ([4]TCOF), the benzo[*c*]naphtho[2,1-*p*]chrysenes **1a** and **1b**. The synthesis is depicted in Fig. 2a. Suzuki-Miyaura cross-coupling of benzene-1,3,5-triyltriboronic ester<sup>36</sup> **2** with an excess of 4-bromo-1-iodo(prop-1-en-1-yl)benzene **3** yields the tribromide **4** in 86% yield. Photocyclization of **4** in the presence of a stoichiometric oxidant yields the tribrominated benzo[*c*]naphtho[2,1-*p*]chrysene core **1a** in 84%<sup>37</sup>. An aromatic *Finkelstein* reaction gives access to the corresponding triiodinated precursor for [4]TCOF **1b** in 86% yield<sup>38</sup>. Analytically pure samples of **1a** and **1b** suitable for ultrahigh-vacuum (UHV)

deposition were isolated as racemic mixtures of slowly interconverting helical diastereoisomers (*PPP/MMM* and *PPM/MMP*). [4]TCOFs were grown on Au(111)/mica films by sublimation of **1a,b** in UHV onto a clean Au(111) surface held at 297 K. Extended Data Fig. ED1 shows constant-current scanning tunnelling microscopy (STM) topographic images of a sub-monolayer coverage of **1a** and **1b** on Au(111) at  $T = 4$  K. Slow annealing of surfaces decorated with the tribrominated precursor **1a** to 473 K gave rise to highly irregular networks that hint at a competition between the desired *Ullmann*-type coupling of aryl halides along the vertices and the surface catalysed cyclodehydrogenation of methyl groups that establishes the extended zigzag edges in the [4]triangulene core (Extended Data Fig. ED2). In an effort to kinetically decouple these two reaction steps, the *Ullmann*-type C–C coupling and the thermal cyclodehydrogenation, we resorted to the more reactive triiodinated precursor **1b**<sup>39,40</sup>. Molecule-decorated surfaces, >0.9 monolayer (ML) **1b** on Au(111), were first annealed at 333 K for 12 h before slowly raising the surface temperature to 473 K. Fig. 2b shows a representative constant-current scanning tunnelling microscopy (STM) image of a two-dimensional (2D) covalent network of [4]triangulenes on Au(111) revealing a statistical distribution of 5-membered (18%), 6-membered (71%), and 7-membered rings (11%), respectively ( $N = 3512$ , Extended Data Fig. ED3). Long range order of bottom-up synthesized [4]TCOFs resulting from **1b** remains low and crystallinity is confined to small isolated domains (Fig. 2c). Bond-resolved STM (BRSTM) reveals that the 2D covalent network is formed by fully fused equilateral triangles featuring atomically smooth zigzag edges with apparent base length, and  $z$ -height of  $0.85 \text{ nm} \pm 0.01 \text{ nm}$  and  $0.14 \text{ nm} \pm 0.02 \text{ nm}$ , respectively, consistent with the formation of the fully cyclodehydrogenated [4]triangulene core (Fig. 2d, Extended Data Fig. ED4). Large area STM images reveal that the cross-linking in 2D COFs prepared from the triiodinated molecular precursor **1b** almost exclusively (>99%) feature the desired C–C bonding between triangulene vertices (Fig. 2c) rather than unselective fusions involving the highly reactive zigzag edges commonly observed for **1a** (Extended Data Fig. ED2).

The local electronic structure of isolated crystalline domains of [4]TCOF was characterized by differential tunnelling ( $dI/dV$ ) spectroscopy. A typical  $dI/dV$  point spectrum recorded at a position corresponding to the centre and the zigzag edge (see BRSTM image in Fig. 3c) of a [4]triangulene subunit

are depicted in Fig. 3a,b. While  $dI/dV$  point spectra recorded near the centre of a triangulene are featureless, besides a characteristic signature assigned to the Au(111) surface state,  $dI/dV$  spectra recorded along the zigzag edges show eight prominent features in the range between  $-2.0 \text{ V} < V_s < +2.0 \text{ V}$ . Two broad peaks centred at  $V_s = -1.55 \pm 0.02 \text{ V}$  (*Peak 1*) and  $V_s = +1.05 \pm 0.02 \text{ V}$  (*Peak 8*) bracket  $E_F$  and can be assigned to deep-lying (i.e. energetically remote from  $E_F$ ) states in the bulk VB and CB, respectively (Fig. 3d). Fig. 3b shows a magnification of the  $dI/dV$  point spectra taken over a narrower bias range of  $-0.6 \text{ V} < V_s < +0.6 \text{ V}$ . Spectra recorded along the zigzag edge show a distinctive pattern of five peaks (*Peaks 2, 3, 4, 6, and 7*) flanking a sharp dip in the differential tunnelling current centred at  $V_s = 0.00 \pm 0.05 \text{ V}$  (*Feature 5*).  $dI/dV$  maps collected at an imaging bias close to  $V_s = 0.00 \text{ V}$  (Fig. 3g) reveal the structure of a featureless network with contrasts rising barely above the Au(111) background, punctuated only by a bright zero-mode state emanating from a local defect in the [4]TCOF lattice. Above and below the semiconducting gap ( $E_{\text{exp}} \sim 0.20 \text{ eV}$ ) the  $dI/dV$  signal rises sharply towards two steps centred at  $V_s = +0.10 \pm 0.05 \text{ V}$  (*Peak 6*) and  $V_s = -0.10 \pm 0.05 \text{ V}$  (*Peak 4*).  $dI/dV$  imaging of the spatial distribution of the LDOS at energies close to *Peak 6* ( $V_s = +0.15 \text{ V}$  in Fig. 3f) reveals a highly diffuse state at the centre of the [4]triangulene superimposed by dark shaded lobes along the zigzag edges. The unusually diffuse nature of the state around  $V_s = +0.15 \text{ V}$  coincides with a characteristic peak in the Au(111) spectrum suggesting the observed LDOS is a superposition of [4]TCOF and Au states dominated by the background.  $dI/dV$  imaging at the corresponding negative bias  $V_s = -0.15 \text{ V}$  (*Peak 4*, Fig 3h) instead reveals a pattern of four bright lobes lining the zigzag edges of each [4]triangulene subunit. The last lobe on either side is shared between zigzag edges and, together with the last lobe of its neighbour [4]triangulene, forms the junction between adjacent building blocks. Beyond these two steps the  $dI/dV$  signal continues to rise steeply and peaks at  $V_s = +0.30 \pm 0.02 \text{ V}$  (*Peak 7*), and  $V_s = -0.30 \pm 0.02 \text{ V}$  (*Peak 3*) respectively. The unusually narrow peak shape and the large signal intensity at  $V_s = \pm 0.30 \text{ V}$  suggest the features represent the signature of van Hove singularities in the quasiparticle density of states. Differential conductance maps recorded at the corresponding biases show clearly distinctive patterns. At  $V_s = +0.30 \text{ V}$  (*Peak 7*) the LDOS is most intense at the lobes coinciding with the junction between covalently linked [4]triangulenes while the signal along the zigzag edges is only

slightly weaker. At  $V_s = -0.30$  V (*Peak 3*) the signal intensity almost uniformly distributed along the four lobes lining the zigzag edge. The last notable feature is a peak at  $V_s = -0.52$  V (*Peak 2*). The corresponding differential conductance maps are reminiscent of the spatial LDOS distribution associated with *Peak 3* and are likely associated with the same band.  $dI/dV$  point spectra recorded directly above the C–C bond linking two adjacent [4]triangulene subunits qualitatively mirror the number and position of peaks recorded along the zigzag edges. STS experiments performed using a variety of CO functionalized STM tips on a set of structurally unique [4]TCOF domains faithfully reproduce the position and intensity of all four key spectral features (*Peaks 3,4,6,7*) straddling a semiconducting gap (*Feature 5*) (Extended Data Fig. ED5,6).

To explore theoretically the electronic ground state of [4]TCOFs we evaluated two distinct models. First, we attempt to describe the electronic structure of a [4]TCOF using conventional *ab initio* density functional theory (DFT) in the local density approximation (LDA). In a second approach we consider a correlated ground state of  $e^-h^+$  pairs within a BCS-like framework, thus allowing for a mixing of VB and CB wavefunction characters in the quasiparticle states of an EI. The DFT-LDA quasiparticle band structure for the six bands closest to the band gap along with the calculated density of states (DOS) of the [4]TCOF are depicted in Fig. 4a and 4b, respectively. Two narrow bands (denoted CFB and VFB) bracket  $E_F$ , enclosing a conventional semiconducting gap of  $E_g \sim 200$  mV. Both bands are virtually dispersionless. The two FBs and the two band complexes can be fit by a TB model (Eq. 1) with  $t_1 = -0.132$  eV,  $t_2 = -0.013$  eV  $t_3 = -0.016$  eV (Fig. 4a, dashed lines). Above and below the conduction and valence FBs, the two pairs of dispersive bands complete the TB picture of a ying-yang Kagome superlattice. On either side of  $E_F$ , the DFT-LDA DOS shows the onset of two sharp features centred at  $E - E_F = \pm 0.10$  eV that extend into a series of smaller peaks at higher and lower energy for the CB and VB complex, respectively. Figs. 4c,d show the square of the theoretical wavefunction amplitude maps at a distance of 4 Å above the plane of a freestanding [4]TCOF at energies corresponding to the valence and the conduction FB edges. Both LDOS maps show distinctive nodal patterns, two bright spots lining the zigzag edges for the CB (Fig. 4c) and two bright spots at the position of the junction between two [4]triangulenes for the VB (Fig. 4d). The corresponding experimental  $dI/dV$  maps (Fig. 4e,f, Extended Data Fig. ED5,6) recorded on pristine [4]TCOF domains at

$V_s = \pm 0.10$  V instead both show a uniform distribution of the wavefunction amplitude shared along the zigzag edges and the junction interface. The obvious mismatch between DFT-LDA LDOS predictions for CB and VB edge states (Fig. 4c,d) and the experimental STS mapping (Fig. 4e,f) suggests that a conventional band insulating ground state given by DFT-LDA is insufficient to describe the electronic structure of [4]TCOF.

In formal analogy to the BCS theory of superconductivity, following Kohn<sup>1</sup>, we derive a second model that describes the transition from a band insulator to an EI for the [4]TCOF ground state and arrive at a theory for the quasiparticle spectrum that is measured in STS (see Methods). Given a semiconducting gap  $E_{\text{exp}} \sim 0.20$  eV (derived from STS) and a triplet exciton eigenenergy  $E_{\text{ex}} = -0.17$  eV (derived from *GW*-BSE)<sup>15</sup>, a resulting finite order parameter  $|\Delta| \sim 0.1$  eV gives rise to a EI ground state at finite temperatures  $T < T_c$ . The corresponding quasiparticle excitations yield in a nearly equal contribution in orbital character from both the conventional VB and CB states. Fig. 4g shows the calculated LDOS map arising from a 1:1 (VB:CB) mixing. The characteristic nodal pattern — four bright lobes lining the zigzag edges, the first and last lobe are shared between adjacent [4]triangulenes — is consistent with the experimental differential conductance maps recorded at  $V_s = \pm 0.10$  V (Figs. 4e,f), corroborating the emergence of an EI ground state. Even for minor changes in the BCS order parameter  $|\Delta|$ , i.e. a slightly reduced contribution to the mixing of VB and CB in Fig. 4h (2:3) and 4i (3:2), the quasiparticle LDOS continue to return a better correspondence to the experimental  $dI/dV$  maps of [4]TCOF (Fig 4e and 4f, respectively) than the band insulator results that do not account for strong  $e^-h^+$  correlations.

Our experimental and theoretical results thus provide strong evidence for the emergence of a flat-band induced EI ground state in a [4]TCOF Kagome lattice at  $T = 4$  K and are based on a detailed investigation of the quasiparticle spectral features in both energy and space. Reticular bottom-up approaches not only provide a general strategy for accessing and exploring other strongly correlated phenomena, but give rise to an expanding class of engineered quantum materials that can deliver further and deeper insights into the crossover between BCS and BEC theory.



## References

- 1 Jerome, D., Rice, T. M. & Kohn, W. Excitonic Insulator. *Phys. Rev.* **158**, 462-475, (1967).
- 2 Kohn, W. Excitonic Phases. *Phys. Rev. Lett.* **19**, 439-442, (1967).
- 3 Cercellier, H. *et al.* Evidence for an excitonic insulator phase in 1T-TiSe<sub>2</sub>. *Phys. Rev. Lett.* **99**, 146403, (2007).
- 4 Wakisaka, Y. *et al.* Excitonic Insulator State in Ta<sub>2</sub>NiSe<sub>5</sub> Probed by Photoemission Spectroscopy. *Phys. Rev. Lett.* **103**, 026402, (2009).
- 5 Lu, Y. F. *et al.* Zero-gap semiconductor to excitonic insulator transition in Ta<sub>2</sub>NiSe<sub>5</sub>. *Nat. Commun.* **8**, 14408, (2017).
- 6 Du, L. J. *et al.* Evidence for a topological excitonic insulator in InAs/GaSb bilayers. *Nat. Commun.* **8**, 1971, (2017).
- 7 Kogar, A. *et al.* Signatures of exciton condensation in a transition metal dichalcogenide. *Science* **358**, 1315-1317, (2017).
- 8 Li, Z. *et al.* Possible Excitonic Insulating Phase in Quantum-Confined Sb Nanoflakes. *Nano Lett.* **19**, 4960-4964, (2019).
- 9 Fukutani, K. *et al.* Electrical Tuning of the Excitonic Insulator Ground State of Ta<sub>2</sub>NiSe<sub>5</sub>. *Phys. Rev. Lett.* **123**, 206401, (2019).
- 10 Sun, B. S. *et al.* Evidence for equilibrium exciton condensation in monolayer WTe<sub>2</sub>. *Nat. Phys.* **18**, 94-99, (2022).
- 11 Jia, Y. Y. *et al.* Evidence for a monolayer excitonic insulator. *Nat. Phys.* **18**, 87-93, (2022).
- 12 Gu, J. *et al.* Dipolar excitonic insulator in a Moiré lattice. *Nat. Phys.* **18**, 395-400, (2022).
- 13 Cheng, Y. *et al.* Light-induced dimension crossover dictated by excitonic correlations. *Nat. Commun.* **13**, 963, (2022).
- 14 Mishra, S. *et al.* Synthesis and Characterization of  $\pi$ -Extended Triangulene. *J. Am. Chem. Soc.* **141**, 10621-10625, (2019).

- 15 Sethi, G., Zhou, Y. N., Zhu, L. H., Yang, L. & Liu, F. Flat-Band-Enabled Triplet Excitonic Insulator in a Diatomic Kagome Lattice. *Phys. Rev. Lett.* **126**, 196403, (2021).
- 16 Bronold, F. X. & Fehske, H. Possibility of an excitonic insulator at the semiconductor-semimetal transition. *Phys Rev B* **74**, 165107, (2006).
- 17 Zenker, B., Ihle, D., Bronold, F. X. & Fehske, H. Electron-hole pair condensation at the semimetal-semiconductor transition: A BCS-BEC crossover scenario. *Phys Rev B* **85**, 121102, (2012).
- 18 Zhou, Y. N., Sethi, G., Liu, H., Wang, Z. F. & Liu, F. Excited quantum anomalous and spin Hall effect: dissociation of flat-bands-enabled excitonic insulator state. *Nanotechnology* **33**, 415001, (2022).
- 19 Mott, N. F. The Transition to the Metallic State. *Philos. Mag.* **6**, 287-309, (1961).
- 20 Halperin, B. I. & Rice, T. M. Possible Anomalies at a Semimetal-Semiconductor Transition. *Rev. Mod. Phys.* **40**, 755-766, (1968).
- 21 Seki, K. *et al.* Excitonic Bose-Einstein condensation in Ta<sub>2</sub>NiSe<sub>5</sub> above room temperature. *Phys Rev B* **90**, 155116, (2014).
- 22 Bucher, B., Steiner, P. & Wachter, P. Excitonic Insulator Phase in TmSe<sub>0.45</sub>Te<sub>0.55</sub>. *Phys. Rev. Lett.* **67**, 2717-2720, (1991).
- 23 Jiang, Z. Y., Li, Y. C., Zhang, S. B. & Duan, W. H. Realizing an intrinsic excitonic insulator by decoupling exciton binding energy from the minimum band gap. *Phys Rev B* **98**, 081408, (2018).
- 24 Jiang, Z. Y. *et al.* Spin-Triplet Excitonic Insulator: The Case of Semihydrogenated Graphene. *Phys. Rev. Lett.* **124**, 166401, (2020).
- 25 Mazzone, D. G. *et al.* Antiferromagnetic excitonic insulator state in Sr<sub>3</sub>Ir<sub>2</sub>O<sub>7</sub>. *Nat. Commun.* **13**, 913, (2022).
- 26 Ma, X. B. *et al.* Ta<sub>2</sub>NiSe<sub>5</sub>: A candidate topological excitonic insulator with multiple band inversions. *Phys Rev B* **105**, 035138, (2022).
- 27 Kohn, W. & Sherrington, D. Two Kinds of Bosons and Bose Condensates. *Rev. Mod. Phys.* **42**, 1-11, (1970).

- 28 Phan, V. N., Becker, K. W. & Fehske, H. Spectral signatures of the BCS-BEC crossover in the excitonic insulator phase of the extended Falicov-Kimball model. *Phys Rev B* **81**, 205117, (2010).
- 29 Rizzo, D. J. *et al.* Inducing metallicity in graphene nanoribbons via zero-mode superlattices. *Science* **369**, 1597-1603, (2020).
- 30 Fu, H. X., Wang, L. W. & Zunger, A. Excitonic exchange splitting in bulk semiconductors. *Phys Rev B* **59**, 5568-5574, (1999).
- 31 Perebeinos, V., Tersoff, J. & Avouris, P. Radiative lifetime of excitons in carbon nanotubes. *Nano Lett.* **5**, 2495-2499, (2005).
- 32 del Aguila, A. G., Groeneveld, E., Maan, J. C., Donega, C. D. & Christianen, P. C. M. Effect of Electron-Hole Overlap and Exchange Interaction on Exciton Radiative Lifetimes of CdTe/CdSe Heteronanocrystals. *ACS Nano* **10**, 4102-4110, (2016).
- 33 Nirmal, M. *et al.* Observation of the Dark Exciton in CdSe Quantum Dots. *Phys. Rev. Lett.* **75**, 3728-3731, (1995).
- 34 Norris, D. J., Efros, A. L., Rosen, M. & Bawendi, M. G. Size dependence of exciton fine structure in CdSe quantum dots. *Phys Rev B* **53**, 16347-16354, (1996).
- 35 Rohlfing, M. & Louie, S. G. Electron-hole excitations and optical spectra from first principles. *Phys Rev B* **62**, 4927-4944, (2000).
- 36 Liu, Y. W., Niu, F. F., Lian, J. R., Zeng, P. J. & Niu, H. B. Synthesis and properties of starburst amorphous molecules: 1,3,5-Tris(1,8-naphthalimide-4-yl)benzenes. *Synthetic Metals* **160**, 2055-2060, (2010).
- 37 Liu, L. B., Yang, B. W., Katz, T. J. & Poindexter, M. K. Improved Methodology for Photocyclization Reactions. *J. Org. Chem.* **56**, 3769-3775, (1991).
- 38 Klapars, A. & Buchwald, S. L. Copper-catalyzed halogen exchange in aryl halides: An aromatic Finkelstein reaction. *J. Am. Chem. Soc.* **124**, 14844-14845, (2002).
- 39 Batra, A. *et al.* Probing the mechanism for graphene nanoribbon formation on gold surfaces through X-ray spectroscopy. *Chem. Sci.* **5**, 4419-4423, (2014).

- 40 Bronner, C. *et al.* Hierarchical On-Surface Synthesis of Graphene Nanoribbon Heterojunctions. *ACS Nano* **12**, 2193-2200, (2018).
- 41 *QUANTUM ESPRESSO*, <<https://www.quantum-espresso.org/>> (2021).
- 42 *BerkeleyGW*, <<https://www.berkeleygw.org/>> (2021).
- 43 Wang, S. K., Zhu, J. M., Blackwell, R. & Fischer, F. R. Automated Tip Conditioning for Scanning Tunneling Spectroscopy. *J. Phys. Chem. A* **125**, 1384-1390, (2021).
- 44 Bartels, L., Meyer, G. & Rieder, K. H. Controlled vertical manipulation of single CO molecules with the scanning tunneling microscope: A route to chemical contrast. *Appl. Phys. Lett.* **71**, 213-215, (1997).
- 45 Giannozzi, P. *et al.* QUANTUM ESPRESSO: a modular and open-source software project for quantum simulations of materials. *J. Phys. Condens. Mat.* **21**, 395502, (2009).
- 46 Deslippe, J. *et al.* BerkeleyGW: A massively parallel computer package for the calculation of the quasiparticle and optical properties of materials and nanostructures. *Comput. Phys. Commun.* **183**, 1269-1289, (2012).
- 47 Hybertsen, M. S. & Louie, S. G. Electron Correlation in Semiconductors and Insulators - Band-Gaps and Quasi-Particle Energies. *Phys Rev B* **34**, 5390-5413, (1986).

## Acknowledgements

This work was primarily funded by the U.S. Department of Energy (DOE), Office of Science, Basic Energy Sciences (BES), Materials Sciences and Engineering Division under Contract No. DE-AC02-05-CH11231 (Nanomachine program KC1203) (molecular design, surface growth, and DFT/GW-BSE calculations). The STM characterization was supported by the U.S. Department of Defense (DOD), Office of Naval Research (ONR) under award no. N00014-19-1-2503, STS analysis by the National Science Foundation (NSF) under award no. CHE-2203911, and spectral signatures of excitonic insulators by the National Science Foundation (NSF) under award no. DMR-1926004. Part of this research program was generously supported by the Heising-Simons Faculty Fellows Program at UC Berkeley. STM instruments are supported in part by the U.S. Department of Defense (DOD), Office of Naval Research (ONR) under award no. N00014-20-1-2824.

Advanced codes are supported by the Center for Computational Study of Excited-State Phenomena in Energy Materials (C2SEPEM), which is funded by the U.S. Department of Energy, Office of Science, Basic Energy Sciences, Materials Sciences and Engineering Division under Contract No. DE-AC02-05CH11231, as part of the Computational Materials Sciences Program. This research used resources of the National Energy Research Scientific Computing Center (NERSC), a U.S. Department of Energy Office of Science User Facility operated under Contract No. DE-AC02-05CH11231. Computational resources were also provided by the NSF TACC Frontera and NSF through ACCESS resources at the NICS (stampede2). C.D. acknowledges support through a Postdoctoral Fellowship funded by the Deutsche Forschungsgemeinschaft (DFG, German Research Foundation) No. 468624869. We thank Dr. Hasan Çelik and UC Berkeley's NMR facility in the College of Chemistry (CoC-NMR) for assistance with spectroscopic characterization. Instruments in the CoC-NMR are supported in part by National Institutes of Health (NIH) award no. S10OD024998.

### **Author Contributions**

A.D., C.D., J.J., S.G.L., and F.R.F. initiated and conceived the research. C.D. and F.R.F. designed, synthesized, and characterized the molecular precursors. A.D., A.C., and F.R.F. performed on-surface synthesis and STM characterization and analysis. J.J. and S.G.L. developed the theory for the spectral signatures of EI, performed DFT and GW/GW-BSE calculations, as well as assisted with data interpretation. A.D., C.D., J.J., S.G.L., and F.R.F. wrote the manuscript. All authors contributed to the scientific discussion.

### **Author Information**

The Reprints and permissions information is available at [www.nature.com/reprints](http://www.nature.com/reprints). The authors declare no competing financial interests. Correspondence and requests for materials should be addressed to [ffischer@berkeley.edu](mailto:ffischer@berkeley.edu) or [sglouie@berkeley.edu](mailto:sglouie@berkeley.edu).

## Main Figure Legends

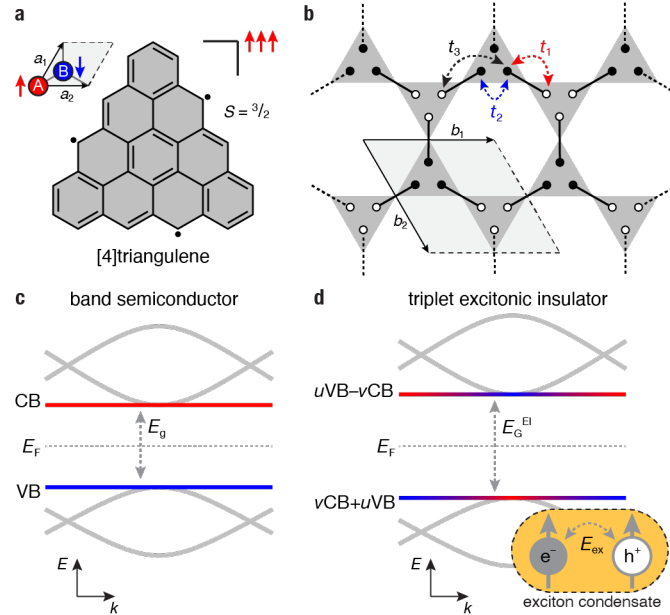


**Figure 1 | Flat-band induced triplet excitonic insulator ground state in a [4]triangulene Kagome**

**lattice. a**, Valence bond model representation of the quartet ( $S = 3/2$ ) ground-state of [4]triangulene. Unit-cell and lattice vectors ( $a_1, a_2$ ) of spin-polarized bipartite lattice of graphene is provided for reference. **b**, Diatomic Kagome lattice spanned by [4]triangulene dimers (unit-cell shaded in grey, lattice vectors  $b_1, b_2$ ). Filled and open circles represent excess up or down electron spins arising from the lattice imbalance at each [4]triangulene superatom site  $\Delta N = N_A - N_B$ .  $t_1, t_2$ , and  $t_3$  are tight-binding hopping amplitudes. **c**, Schematic representation of the band structure of a flat-band conventional semiconductor ground-state. **d**, Schematic representation of the band structure of a triplet excitonic insulator ground-state.  $E_g, E_G^{EI}$ , and  $E_{ex}$  are the semiconducting band gap, the new quasiparticle gap in the EI state, and the exciton energy, respectively. Colour gradient in  $uVB-vCB$  and  $vCB+uVB$  represents the mixing of characters of the valence (blue) and conduction (red) flat-bands (of the conventional band insulator) in the excitonic insulator quasiparticle states ( $u$  and  $v$  are the respective mixing coefficients, see Methods for derivation). BEC formed by triplet excitons shaded in orange indicates the property of the EI ground state and should not be viewed as a part of the quasiparticle band structure.

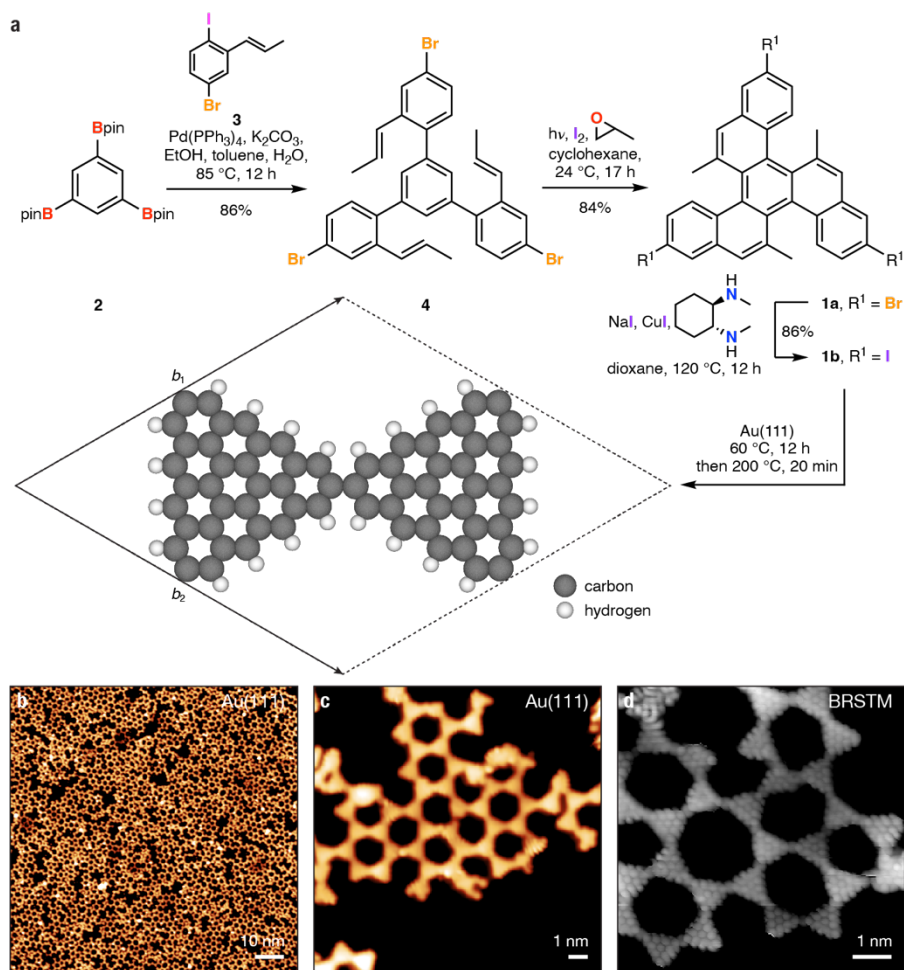


**Figure 2 | Bottom-up synthesis of [4]TCOF Kagome lattice. a**, Schematic representation of the bottom-up synthesis and on-surface growth of [4]TCOFs from molecular precursors **1a,b**. **b**, STM topographic image of 2D covalent network of [4]triangulenes on Au(111) ( $V_s = 200$  mV,  $I_t = 20$  pA). **c**, STM topographic image of a segment of the Kagome lattice of [4]TCOF ( $V_s = 50$  mV,  $I_t = 20$  pA). **d**, BRSTM topographic image of fully cyclodehydrogenated [4]TCOF segment showing the C–C bonding between vertices of triangulenes along with the characteristic zigzag edges of [4]triangulene building blocks ( $V_s = 10$  mV,  $I_t = 400$  pA). All STM experiments performed at  $T = 4$  K.

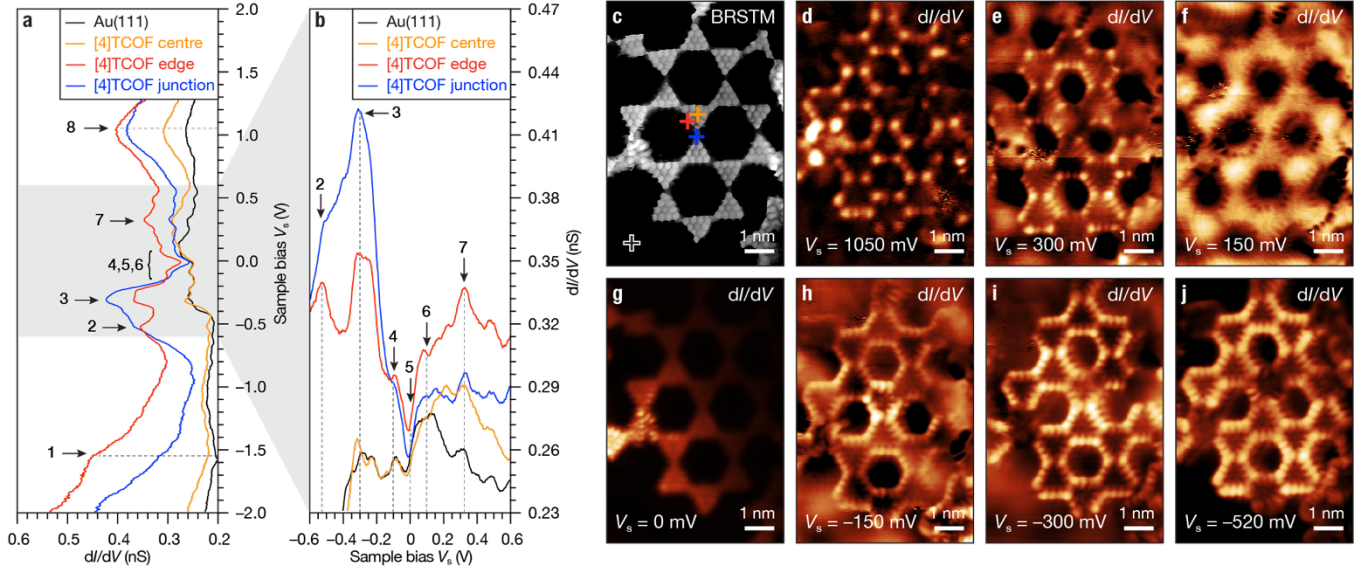


**Figure 3 | Electronic structure of [4]TCOF.** **a–b**,  $dI/dV$  point spectra of [4]TCOF/Au(111) recorded at the position marked in (c) (Au(111) surface state, black; centre of [4]triangulene, orange; zigzag edge of [4]triangulene, red; junction between two [4]triangulene units, blue;  $V_{ac} = 10$  mV,  $f = 455$  Hz, CO-functionalized tip). **c**, Constant-height BRSTM image of [4]TCOF/Au(111) segment ( $V_s = 0$  mV,  $V_{ac} = 10$  mV,  $f = 455$  Hz, CO-functionalized tip). Crosses mark the position of where  $dI/dV$  point spectra were recorded. **d–j**, Constant-current  $dI/dV$  maps recorded at a voltage bias of  $V_s = +1050$  mV,  $V_s = +300$  mV,  $V_s = +150$  mV,  $V_s = +0$  mV,  $V_s = -150$  mV,  $V_s = -300$  mV, and  $V_s = -520$  mV ( $V_{ac} = 10$  mV,  $I_t = 400$  pA,  $f = 455$  Hz, CO-functionalized tip). All STM experiments performed at  $T = 4$  K.



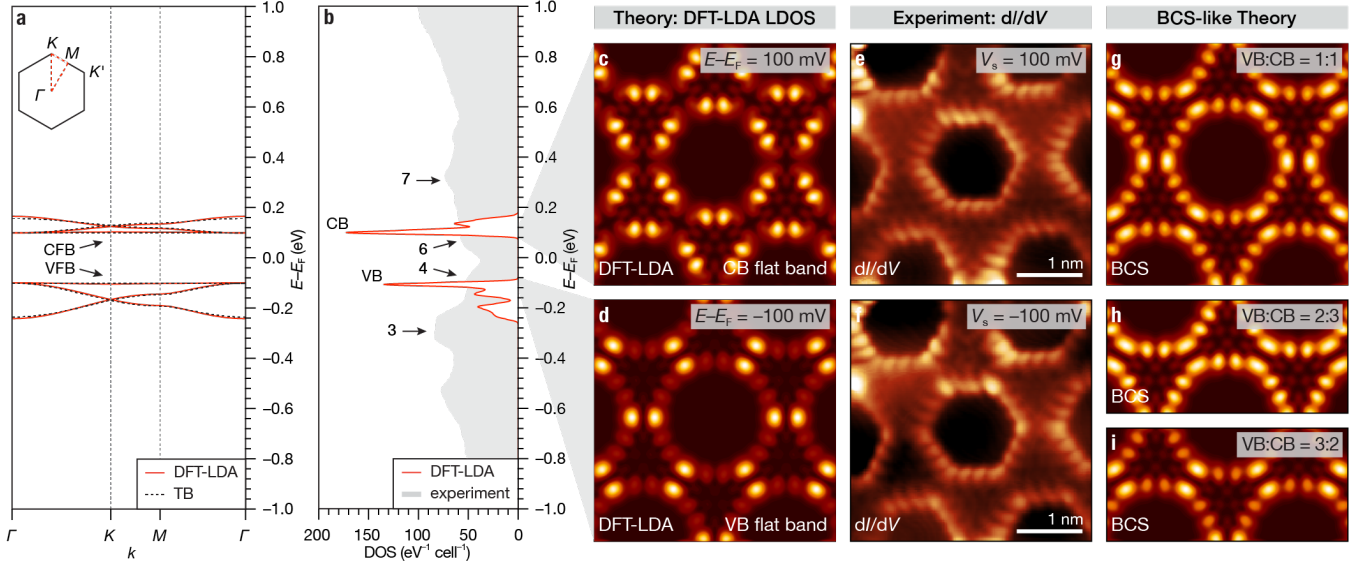


**Figure 4 | Quasiparticle states from DFT and BCS-EI calculations in [4]TCOFs.** **a**, DFT-LDA band structure for six bands near  $E_F$  of a freestanding [4]TCOF. Valence (VB) and conduction (CB) flat-bands are indicated by arrows. **b**, Calculated DFT-LDA LDOS at 4 Å above a freestanding [4]TCOF (spectrum broadened by 10 meV Gaussian). Experimental  $dI/dV$  point spectrum recorded along a zigzag edge is overlaid in grey. **c**, Calculated DFT-LDA LDOS map evaluated at the edge of the conduction flat-band (CFB). **d**, Calculated DFT-LDA LDOS map evaluated at the edge of the valence flat-band (VFB). **e**, Experimental constant-current  $dI/dV$  maps recorded at a voltage bias of  $V_s = +100$  mV ( $V_{ac} = 10$  mV,  $I_t = 400$  pA,  $f = 455$  Hz, CO-functionalized tip). **f**, Experimental constant-current  $dI/dV$  maps recorded at a voltage bias of  $V_s = -100$  mV ( $V_{ac} = 10$  mV,  $I_t = 400$  pA,  $f = 455$  Hz, CO-functionalized tip). **g**, Calculated LDOS map resulting from a BCS-like 1:1 mixing of character of the VB and CB flat bands for quasiparticles in the EI phase. **h–i**, Calculated EI quasiparticle LDOS map resulting from a BCS-like 2:3 and 3:2 mixing of character of the VB and CB flat bands, respectively. All STM experiments performed at  $T = 4$  K.

## Data Availability

DFT code with pseudopotentials and GW code can be downloaded from the Quantum Espresso<sup>41</sup> and the BerkeleyGW<sup>42</sup> website, respectively. For this study we used Quantum Espresso version 6.7 and BerkeleyGW version 3.0 for the theoretical calculations. All data presented in the main text and the supplementary materials are available from the corresponding authors upon reasonable request.

## Methods

**Precursor Synthesis and [4]TCOF Growth.** Full details of the synthesis and characterization of **1a,b** are given in the Supplementary Information. [4]TCOF were grown on Au(111)/mica films under UHV conditions. Atomically clean Au(111) surfaces were prepared through iterative Ar<sup>+</sup> sputter/anneal cycles. 0.9 ML coverage of **1a,b** on atomically clean Au(111) was obtained by sublimation at crucible temperatures of 463–473 K using a home-built Knudsen cell evaporator. After deposition the surface temperature was held at 333 K for 12 h before slowly ramping ( $\leq 2 \text{ K min}^{-1}$ ) to 473 K and held at this temperature for 20 min.

**STM Measurements.** All STM experiments were performed using a commercial OMICRON LT-STM operating at  $T = 4 \text{ K}$  using PtIr STM tips. STM tips were optimized for scanning tunnelling spectroscopy using an automated tip conditioning program<sup>43</sup>.  $dI/dV$  measurements were recorded with CO-functionalized STM tips<sup>44</sup> using a lock-in amplifier with a modulation frequency of 455 Hz and a modulation amplitude of  $V_{\text{RMS}} = 10 \text{ mV}$ .  $dI/dV$  point spectra were recorded under open feedback loop conditions.  $dI/dV$  maps were collected under constant current conditions. BRSTM images were obtained by mapping the out-of-phase  $dI/dV$  signal collected during a constant-height  $dI/dV$  map at zero bias. Peak positions in  $dI/dV$  point spectroscopy were determined by fitting the spectra with Lorentzian peaks. Peak positions are calibrated to the Au(111) Shockley surface state.

**Calculations.** DFT calculations were performed in the LDA as implemented in the Quantum ESPRESSO package<sup>45</sup>, and the GW calculations were performed with the BerkeleyGW package<sup>46</sup>. A supercell arrangement was used to simulate an isolated 2D material with 15 Å-wide vacuum gap along the direction normal to the atomic plane, and carefully tested to avoid interactions between the 2D lattice

and its periodic images. We used norm-conserving pseudopotentials with a planewave energy cut-off of 60 Ry. The structure was fully relaxed within DFT-LDA until the magnitude of the force on each atom was smaller than 0.01 eV Å<sup>-1</sup>. All  $\sigma$  dangling bonds on the edges of the triangulenes forming the [4]TCOF were capped by hydrogen atoms. A Gaussian broadening of 10 meV was used in the evaluation of the DOS. In the  $GW$  calculation, the frequency-dependent screening is incorporated by the Hybertsen-Louie GPP model<sup>47</sup>.

**BCS-like Theory for Excitonic Insulator in the Flat-Bands Model.** Starting from the gap equation of an EI<sup>1</sup>

$$\Delta_{cvk} = -\sum_{c'v'k'} V_{cvk,c'v'k'} \frac{\Delta_{c'v'k'}}{2E_{c'v'k'}}, \quad (2)$$

where  $c, v, c', v'$  are the CB and VB indexes,  $\mathbf{k}, \mathbf{k}'$  indicate the  $\mathbf{k}$ -points, and  $V$  is the screened Coulomb attraction potential between electron and hole in a triplet exciton state. Since the CFB and VFB have little dispersion near the  $E_F$ , we can drop the  $c, v, \mathbf{k}$  dependence of the order parameter and study the averaged effect across the gap.  $E_{cvk} \rightarrow E = \sqrt{\xi^2 + |\Delta|^2}$  with  $\xi = \frac{1}{2}(\epsilon_{CB} - \epsilon_{VB})$  where  $\epsilon_{CB}$  and  $\epsilon_{VB}$  are the CB and VB energies of the band insulator state, respectively. The effective quasiparticle gap  $E_G^{\text{EI}}$  in the EI state is given by  $E_G^{\text{EI}} = 2E$ .

With  $\frac{\Delta}{E_G^{\text{EI}}}$  defined as  $\chi$ , we can rewrite equation (2) as:

$$E_G^{\text{EI}} \chi = -\sum_{c'v'k'} V_{cvk,c'v'k'} \chi. \quad (3)$$

From the Bethe–Salpeter equation (BSE)<sup>35</sup> for excitons from flat bands we have

$$(2\xi - E_{\text{ex}})A = -\sum_{c'v'k'} V_{cvk,c'v'k'} A \quad (4)$$

where  $E_{\text{ex}}$  is the exciton eigenenergy. Comparing equation (3) and (4), we arrive at:

$$E_G^{\text{EI}} = (2\xi - E_{\text{ex}}). \quad (5)$$

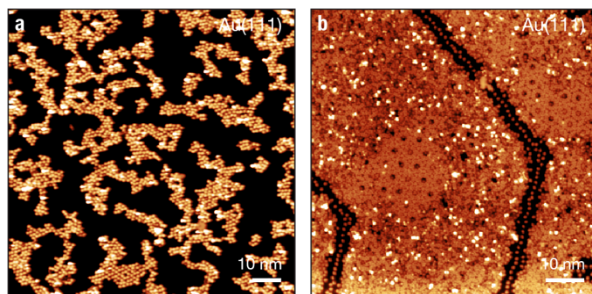
This means that only if  $E_{\text{ex}} < 0$ , a nonzero solution for  $\Delta$  is possible. During the STS experiment, the [4]TCOF Kagome lattice is adsorbed on a gold substrate. Since the exciton eigenenergy is insensitive to screening by the environment, we can approximate  $E_{\text{ex}}$  from calculations on an isolated [4]TCOF Kagome

lattice. *GW*-BSE gives an exciton eigenenergy of  $E_{\text{ex}} = -0.17 \text{ eV}^{15}$ . Given the experimental semiconducting gap  $E_{\text{exp}}$  determined by the peak-to-peak distance in the STS experiments, we can substitute  $E_{\text{G}}^{\text{EI}} = E_{\text{exp}} \sim 0.20 \text{ eV}$ . Equation (5) then gives an effective band gap in the band insulator phase of the [4]TCOF Kagome lattice of  $2\xi = 0.03 \text{ eV}$ . This yields a  $|\Delta| = 0.1 \text{ eV}$  and  $|u| \sim |v|$  in the BCS ground state:

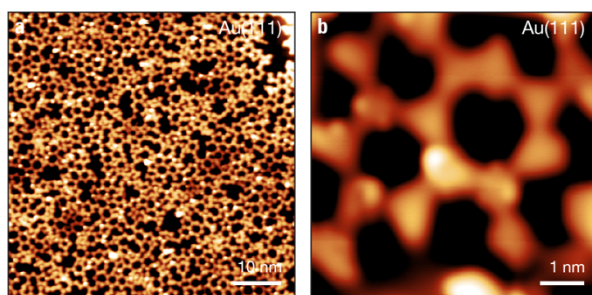
$$|G\rangle = \prod_{vck} (u + v c_{ck}^\dagger c_{vk}) |\Phi\rangle. \quad (6)$$

Here  $|\Phi\rangle$  is the normal ground state with all VBs occupied and CBs empty, with  $|u|^2 = \frac{1}{2} \left(1 + \frac{\xi}{E}\right)$ ,  $|v|^2 = \frac{1}{2} \left(1 - \frac{\xi}{E}\right)$  obtained from the BCS-like theory. The quasiparticle excitation then results in an almost equal mixing of both CB and VB characters, which agrees well with our experimental findings.

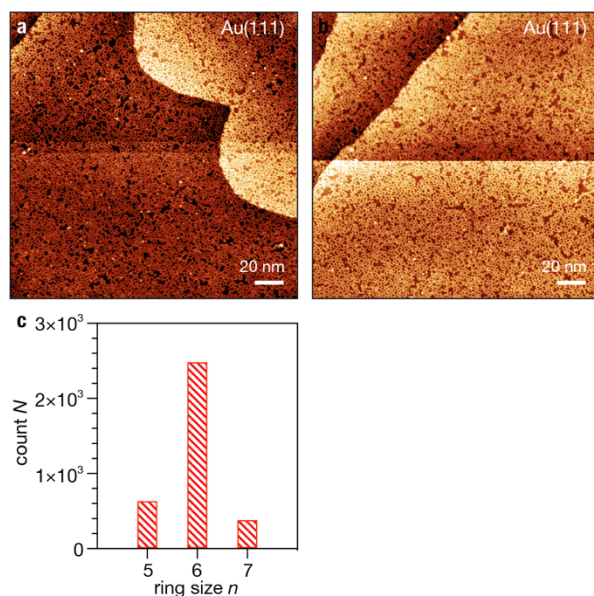
## Extended Data Figure Legends



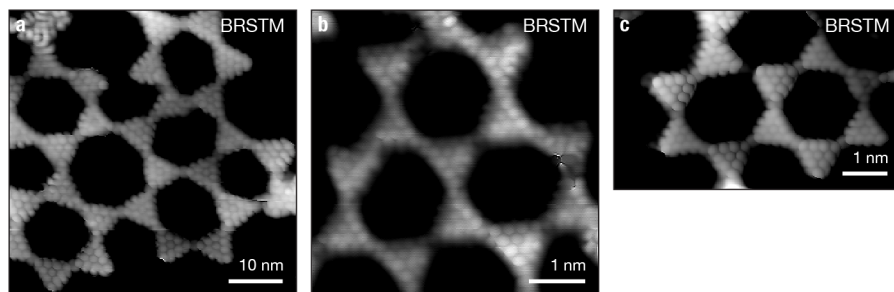
**Extended Data Figure ED1 | Self-assembly of molecular precursors 1a and 1b on Au(111).** **a**, STM topographic image of a sub-monolayer coverage of the brominated molecular precursor **1a** on Au(111) ( $V_s = 600$  mV,  $I_t = 20$  pA). **b**, STM topographic image of a sub-monolayer coverage of the iodinated molecular precursor **1b** on Au(111) ( $V_s = 200$  mV,  $I_t = 20$  pA). All STM experiments performed at  $T = 4$  K.



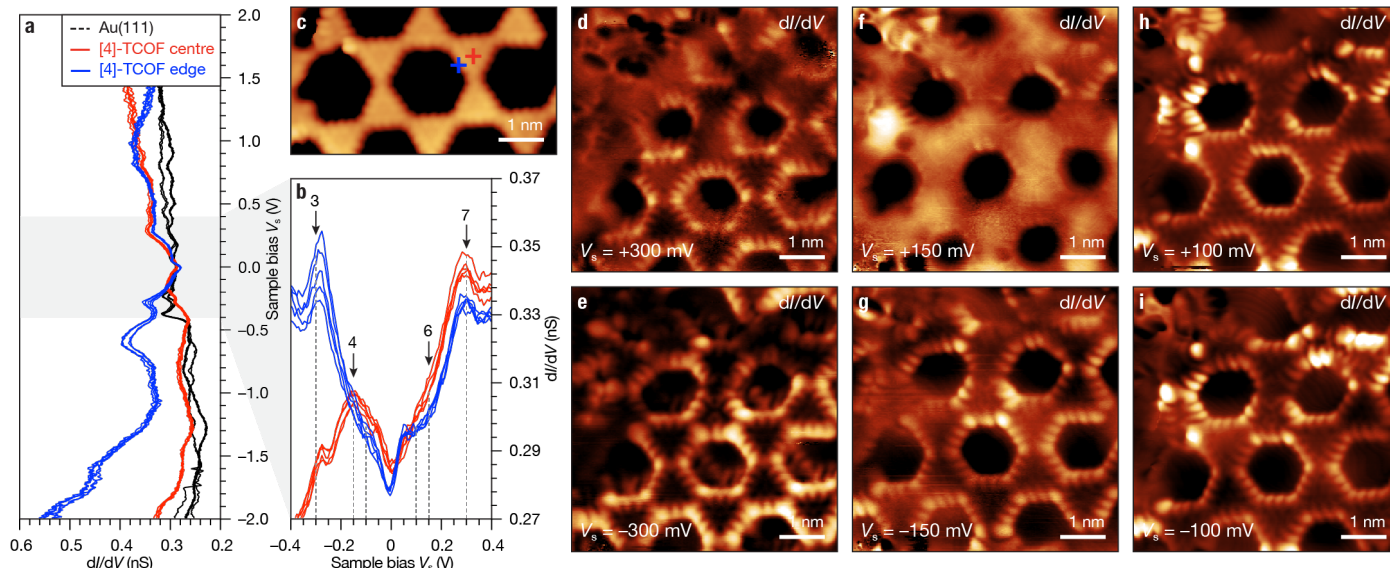
**Extended Data Figure ED2 | On-surface reticular synthesis of 2D networks from brominated molecular precursor 1a.** **a**, STM topographic image of 2D covalent network of [4]triangulenes grown from **1a** on Au(111) ( $V_s = 200$  mV,  $I_t = 20$  pA). **b**, STM topographic image of a representative highly defective segment of the 2D network grown from **1a** showing the cross linkage between corners and along the zigzag edges. ( $V_s = 200$  mV,  $I_t = 20$  pA). All STM experiments performed at  $T = 4$  K.



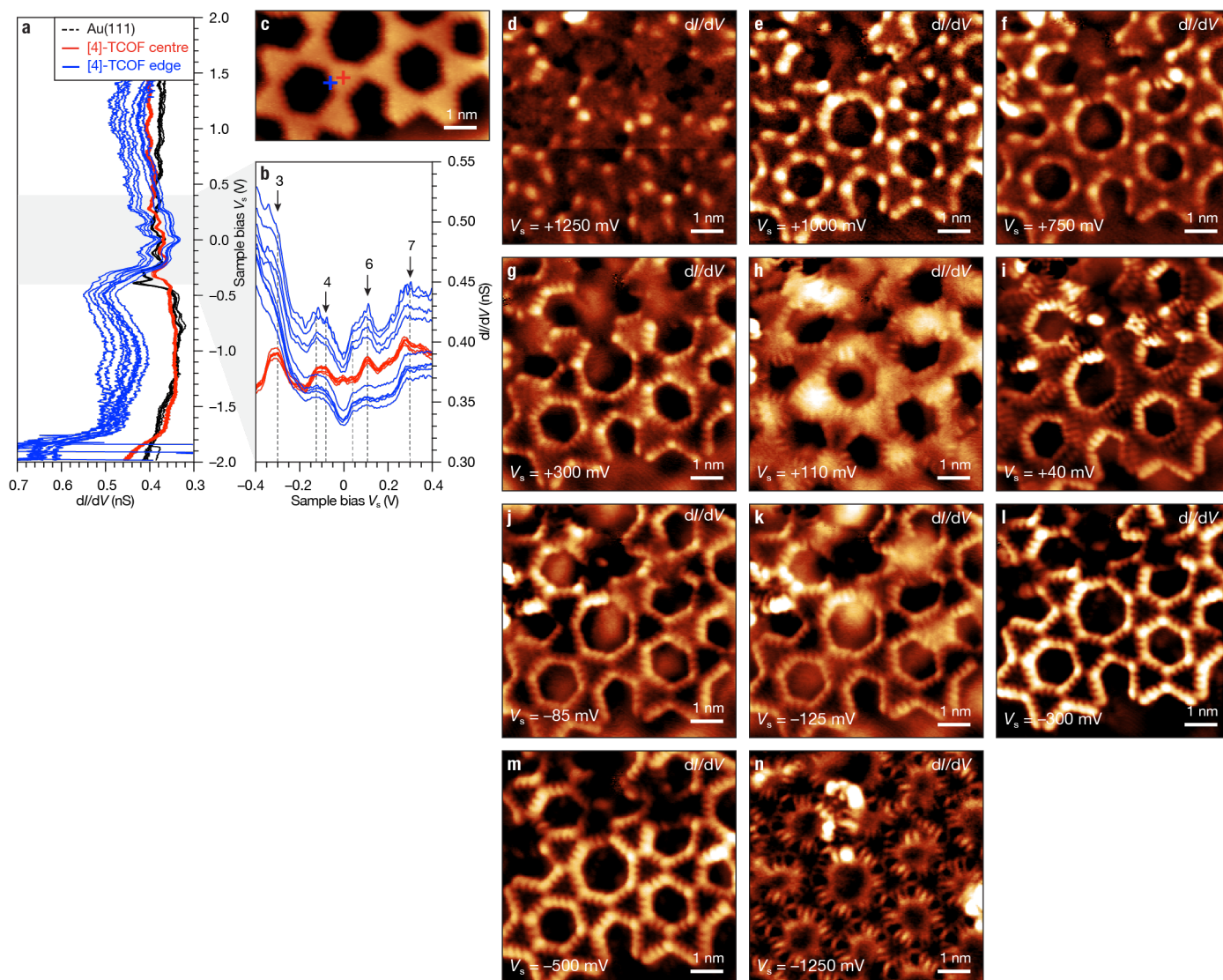
**Extended Data Figure ED3 | Statistical distribution of ring sizes in [4]triangulene COF grown from 1b.** **a,b**, Representative STM topographic images of 2D covalent networks of [4]triangulenes grown from **1b** on Au(111) ( $V_s = 100$  mV,  $I_t = 20$  pA). All STM experiments performed at  $T = 4$  K. **c**, Statistical distribution of  $n$ -membered rings formed by [4]triangulenes in a sample of [4]TCOF grown from **1b** on Au(111) ( $N = 3512$ ).



**Extended Data Figure ED4 | Bond resolved STM imaging of cyclodehydrogenated [4]triangulene building blocks.** **a–d**, Constant-height BRSTM images of [4]TCOF/Au(111) segments ( $V_s = 0$  mV,  $V_{ac} = 10$  mV,  $f = 455$  Hz, CO-functionalized tip). All STM experiments performed at  $T = 4$  K.



**Extended Data Figure ED5 | Electronic structure of [4]TCOF.** **a–b**,  $dI/dV$  point spectra of [4]TCOF/Au(111) recorded at the position marked in (c) (Au(111) surface state, black; centre of [4]triangulene, red; zigzag edge of [4]triangulene, blue;  $V_{ac} = 10$  mV,  $f = 455$  Hz, CO-functionalized tip). **c**, STM topographic image of [4]TCOF/Au(111) segment ( $V_s = 50$  mV,  $I_t = 400$  pA, CO-functionalized tip). Crosses mark the position of where  $dI/dV$  point spectra were recorded. **d–i**, Constant-current  $dI/dV$  maps recorded at a voltage bias of  $V_s = +300$  mV,  $V_s = +150$  mV,  $V_s = +100$  mV,  $V_s = -100$  mV,  $V_s = -150$  mV, and  $V_s = -300$  mV ( $V_{ac} = 10$  mV,  $I_t = 400$  pA,  $f = 455$  Hz, CO-functionalized tip). All STM experiments performed at  $T = 4$  K.



**Extended Data Figure ED6 | Electronic structure of [4]TCOF.** **a–b**,  $dI/dV$  point spectra of [4]TCOF/Au(111) recorded at the position marked in (c) (Au(111) surface state, black; centre of [4]triangulene, red; zigzag edge of [4]triangulene, blue;  $V_{ac} = 10$  mV,  $f = 455$  Hz, CO-functionalized tip). **c**, STM topographic image of [4]TCOF/Au(111) segment ( $V_s = 40$  mV,  $I_t = 400$  pA, CO-functionalized tip). Crosses mark the position of where  $dI/dV$  point spectra were recorded. **d–n**, Constant-current  $dI/dV$  maps recorded at a voltage bias of  $V_s = +1250$  mV,  $V_s = +1000$  mV,  $V_s = +750$  mV,  $V_s = +300$  mV,  $V_s = +110$ ,  $V_s = +40$ ,  $V_s = -85$  mV,  $V_s = -125$  mV,  $V_s = -300$  mV,  $V_s = -500$  mV, and  $V_s = -1250$  mV ( $V_{ac} = 10$  mV,  $I_t = 400$  pA,  $f = 455$  Hz, CO-functionalized tip). All STM experiments performed at  $T = 4$  K.



## Supplementary Information

Supplementary Information contains detailed synthetic procedures and characterization of precursor **1a,b**.